Cooperative regulation of C1-domain membrane recruitment polarizes atypical Protein Kinase C

Kimberly A. Jones*, Michael L. Drummond*, Rhiannon R. Penkert, and Kenneth E. Prehoda

Institute of Molecular Biology
Department of Chemistry and Biochemistry
1229 University of Oregon
Eugene, OR 97403

*Equal contributions

Corresponding author: prehoda@uoregon.edu

Abstract

Recruitment of the Par complex protein atypical Protein Kinase C (aPKC) to a specific membrane domain is a key step in the polarization of animal cells. While numerous proteins and phospholipids interact with aPKC, how these interactions cooperate to control its membrane recruitment has been unknown. Here we identify aPKC's C1 domain as a phospholipid interaction module that targets aPKC to the membrane of *Drosophila* neural stem cells (NSCs). The isolated C1 binds the NSC membrane in an unpolarized manner during interphase and mitosis and is uniquely sufficient among aPKC domains for targeting. Other domains, including the catalytic module and those that bind the upstream regulators Par-6 and Bazooka, restrict C1's membrane targeting activity – spatially and temporally – to the apical NSC membrane during mitosis. Our results suggest that aPKC polarity results from cooperative activation of autoinhibited C1-mediated membrane binding activity.

Introduction

The Par complex polarizes animal cells by excluding specific cortical factors from the Par cortical domain (Lang and Munro, 2017; Venkei and Yamashita, 2018). During polarization the proteins Par-6 and atypical Protein Kinase C (aPKC), which make up the complex, are recruited to a specific, continuous region of the cell membrane, such as the apical surface of epithelia (Tepass, 2012), the anterior hemisphere of the *C. elegans* zygote (Nance and Zallen, 2011), or the apical hemisphere of *Drosophila* neural stem cells (NSCs) (Prehoda, 2009). Factors that are directly polarized by the Par complex, such as Miranda and Numb, are aPKC substrates (Atwood and Prehoda, 2009; Smith et al., 2007). Phosphorylation is coupled to removal from the Par domain, causing these substrates to localize to a complementary membrane domain (Bailey and Prehoda, 2015). Thus, the pattern of Par-polarized factors is ultimately determined by the mechanisms that specify aPKC's membrane recruitment and activation.

Many aPKC interactions with proteins and phospholipids have been identified (Figure 1A), although how they collaborate to polarize aPKC remains poorly understood. Bazooka (Baz aka Par-3) and Par-6 form direct physical contacts with aPKC, and each protein has possible pathways for membrane recruitment: Baz through direct interactions with the membrane and Par-6 through interactions with prenylated Cdc42 (Joberty et al., 2000; Lin et al., 2000; Krahn et al., 2010). Several direct interactions with phospholipids have also been reported, including with ceramide (Wang et al., 2005), sphingosine-1-phosphate (Kajimoto et al., 2019), and phosphoinositides (Dong et al., 2020; Standaert et al., 1997). The aPKC catalytic domain may

also play a role in membrane recruitment as perturbations in this domain can cause aPKC to become depolarized (Rodriguez et al., 2017; Hannaford et al., 2019).

While interactions that could potentially recruit aPKC to the membrane have been identified, what is missing is an understanding of how the interactions function together to polarize aPKC at the proper time. One possibility is an avidity model where each interaction is weak, unable to recruit aPKC to the membrane on its own, but the energy provided by multiple interactions allows for recruitment. Alternately, one or more interactions could be sufficient for recruitment but somehow regulated to ensure that targeting only occurs when the appropriate cues are present. These models could be distinguished by determining if any interactions are sufficient for targeting.

We used *Drosophila* NSCs to investigate how aPKC is recruited to the membrane during polarization (Homem and Knoblich, 2012). During interphase, aPKC is cytoplasmic in NSCs but becomes targeted to the apical hemisphere early in mitosis, ultimately concentrating near the apical pole before depolarizing and returning to the cytoplasm as division completes (Oon and Prehoda, 2019). The highly dynamic nature of the NSC polarity cycle makes it possible to assess both spatial (polarized, depolarized, or cytoplasmic) and temporal (interphase or mitotic) aspects of aPKC membrane recruitment regulation.

Results

Mutations that inactivate catalytic activity depolarize aPKC

We began our examination of aPKC membrane targeting mechanisms in NSCs by evaluating the role of the catalytic domain. At metaphase, aPKC is highly enriched at the apical membrane of larval brain NSCs (Rolls et al., 2003). We examined the effect of mutations that inactivate aPKC's catalytic activity on its localization in cells that lacked endogenous aPKC (*apkc*^{K06403} in positively marked clones; Lee and Luo, 1999). Besides aPKC's localization, we also examined its activity in these metaphase NSCs by determining the localization of Miranda (Mira), an aPKC substrate that is normally restricted to the basal cortex by apical aPKC activity (Figure 1B) (Atwood and Prehoda, 2009; Ikeshima-Kataoka et al., 1997). Consistent with previous observations, we found that in metaphase *apkc*^{K06403} NSCs, Mira was allowed to enter the apical cortex becoming uniformly cortical (Figure 1B). Expression of wild-type aPKC restores the apical aPKC and basal Mira localization found in normally functioning NSCs to positively marked *aPKC*^{K06403} metaphase null clones (Holly et al., 2020).

64 To examine the effect of perturbing catalytic activity, we expressed aPKC harboring a mutation
65 (D388A) that does not have detectable activity in an *in vitro* protein kinase assay (Holly et al.,
66 2019). This mutation is in a residue that coordinates the γ-phosphate of ATP and is thought to
67 allow ATP to bind but prevent phosphotransfer (Cameron et al., 2009). Unlike wild-type aPKC,
68 which is restricted to the apical domain at metaphase, we found that aPKC D388A was largely
69 depolarized, localizing along the entire cortex of positively marked *aPKC*^{K06403} metaphase null
70 clones (Figure 1B). Mira also localized uniformly to the cortex in these cells, confirming that
71 aPKC D388A is inactive both *in vitro* (Holly et al., 2019) and *in vivo* (Figure 1B). We conclude
72 that inactivation of the aPKC catalytic domain depolarizes aPKC in metaphase NSCs.

73 **Kinase inactive aPKC is not polarized by endogenous aPKC**

74 Our results indicate that mutations that perturb aPKC's catalytic activity also influence its
75 localization. Previous examinations of chemically inhibited aPKC also found that perturbing
76 catalytic activity caused aPKC to localize to the membrane but in a depolarized manner
77 (Rodriguez et al., 2017; Hannaford et al., 2019). The depolarization caused by perturbations to
78 the kinase domain could be explained if aPKC's catalytic activity directly participated in its own
79 localization (e.g. by a feedback mechanism). Alternately, perturbations in the kinase domain
80 could alter other aPKC functions. Besides catalyzing phosphotransfer, the aPKC kinase
81 domain also binds a pseudosubstrate in its NH_2-terminal region causing autoinhibition (Graybill
82 et al., 2012). Mutations or small molecules that influence the active site could perturb the
83 intramolecular interaction in addition to inhibiting catalytic activity. To determine whether the
84 loss of aPKC's catalytic activity is responsible for the localization defects of aPKC D388A, we
85 examined whether the presence of wild-type, endogenous aPKC with its normal level of
86 catalytic activity could restore aPKC D388A polarity. We also tested the localization of a well-
87 characterized kinase inactive mutation K293W, which blocks ATP binding (Graybill et al, 2012).
88 In NSCs containing endogenous aPKC, both aPKC D388A and K293W remained enriched at
89 the membrane (Figure 1C,D) but depolarized (Figure 1C,E), indicating that aPKC catalytic
90 activity is not sufficient to restore polarity to these proteins. Interestingly, in cells expressing
91 aPKC K293W Mira was basally polarized but in cells expressing aPKC D388A it was
92 depolarized suggesting that aPKC D388A influences the localization or activity of endogenous
93 aPKC (Figure 1C). We do not know the origin of the differential effects of aPKC K293W and
94 aPKC D388A on Mira localization, but it may arise from differences in the amounts of the two
95 proteins and how endogenous aPKC is affected.

96 We also examined the localization of the aPKC variants during interphase, when membrane-
97 bound aPKC is normally not detectable, and found that the kinase inactivating mutations were
98 predominantly found in the nucleus, presumably due to an embedded nuclear localization
99 signal (Perander et al., 2001; Seidl et al., 2012). However, we also found that the aPKC kinase
100 domains variants were enriched at the membrane relative to the cytoplasm (at sites away from
101 progeny cell contacts) although at a level somewhat lower than apical WT protein at
102 metaphase (Figure 1F,G).

103 Baz and Par-6 are normally found at the apical membrane with aPKC at metaphase. We
104 examined whether the kinase inactive aPKC mutants influence Baz or Par-6 localization (Figure
105 2). We found that Baz remained apically polarized in cells expressing aPKC, as well as those
106 expressing the aPKC D388A or aPKC K293W variants, although the intensity of this crescent
107 was slightly reduced in aPKC D388A (Figure 2A, C). While Baz localization was unperturbed by
108 the expression of the kinase inactive aPKC variants, Par-6 expanded into the basal domain like
109 the localization of aPKC D388A and aPKC K293W (Figure 2A, B). We conclude that expression
110 of kinase inactive aPKC leads to loss of Par-6 polarity but does not influence the localization of
111 Baz. Depolarization of Par-6 but not Baz has also been observed when aPKC was chemically
112 inhibited (Hannaford et al., 2019).

113 **Kinase inactive aPKC may bind the NSC membrane independently of Cdc42 and Bazooka**
114 Membrane targeting of aPKC normally requires the activities of Baz and the small GTPase
115 Cdc42 (Wodarz et al., 2000; Rolls et al., 2003; Atwood et al., 2007). We tested whether these
116 upstream regulators are required for the uniformly cortical localization of kinase inactive aPKC
117 by examining the localization of aPKC K293W in NSCs expressing Baz or Cdc42 RNAi. We
118 found that wild-type aPKC failed to recruit to the membrane in these contexts, as previously
119 reported (Figure 3A-D) (Atwood et al., 2007; Rolls et al., 2003). Consistent with this
120 observation, we found that Mira was depolarized, localizing uniformly to the cortex in these
121 cells. In contrast to wild-type aPKC, however, aPKC K293W was able to remain on the cortex
122 even when Cdc42 was absent (Figure 3A-B). We also examined the localization of the aPKC
123 K293W variant in NSCs expressing Baz RNAi. In this context, less aPKC is recruited to the
124 apical membrane and Mira becomes depolarized as previously reported (Atwood et al., 2007).
125 However, aPKC K293W's remained highly enriched on the membrane (i.e., more than WT
126 aPKC) when Baz was reduced (Figure 3C-D). While we cannot completely exclude a role for
127 Cdc42 and Baz in recruiting aPKC K293W to the membrane, we conclude that aPKC K293W is

128 targeted to the membrane significantly more than WT aPKC in metaphase NSCs with reduced
129 Cdc42 or Baz function.

130 **The aPKC C1 domain is a constitutive membrane targeting module**

131 Our results indicate that the uniform membrane localization of aPKC with inactive kinase
132 domains (e.g., K293W) is independent of both Baz and Cdc42. One model consistent with
133 these results is that aPKC contains a membrane targeting module that is regulated by its
134 kinase domain, along with Baz and Cdc42 binding. To identify the putative module, we first
135 examined whether removing the kinase domain leads to the same uniform membrane
136 localization phenotype. We found that aPKC PB1-C1 (aka ΔKD; Figure 4A) was enriched at the
137 membrane and not polarized (Figure 4B-D). A similar localization pattern has been reported for
138 aPKC PB1-C1 expressed in cultured cells (Dong et al., 2020). Thus, aPKC's NH_2-terminal
139 regulatory region, consisting of PB1, PS, and C1 domains, is responsible for membrane
140 binding. The PB1 could mediate interaction with the membrane via protein-protein interactions
141 with Par-6 (Atwood et al., 2007; Petronczki and Knoblich, 2001), the PS domain through direct
142 interactions with lipids (Dong et al., 2020), or the C1 domain which serves as a membrane
143 targeting module in other PKCs (Colón-González and Kazanietz, 2006) but has not been
144 reported to do so in aPKCs. Removal of the C1 domain from the regulatory domain (aPKC
145 PB1-PS) leaving the PB1 and PS domains (Figure 4A), resulted in a protein that was not
146 enriched at the membrane (Figure 4B-D). Thus, the PB1 and PS domains are not sufficient for
147 membrane targeting in NSCs. We next tested the C1 domain alone and found that it was
148 enriched uniformly to the membrane relative to the cytoplasm (Figure 4B-D). We also observed
149 C1 enrichment at the membrane during interphase (Figure 4E), although the domain was
150 predominantly found in the nucleus, presumably due to an embedded nuclear localization
151 signal (Perander et al., 2001; Seidl et al., 2012). We conclude that the aPKC C1 domain is a
152 membrane targeting module.

153 **C1 is a lipid binding module that is required for aPKC membrane recruitment**

154 How might the C1 domain mediate interaction with the NSC membrane? C1 domains from
155 canonical PKCs bind diacylglycerol (DAG), although the aPKC C1 domain does not bind DAG
156 (Colón-González and Kazanietz, 2006). However, we sought to determine if aPKC's C1 domain
157 binds other phospholipids. We used a vesicle pelleting assay in which Giant Unilamellar
158 Vesicles (GUVs) with varying phospholipid compositions were mixed with purified aPKC C1
159 domain. The vesicles were separated from the soluble phase by ultracentrifugation and any

160 associated C1 was identified by protein gel electrophoresis. We observed varying degrees of
161 C1 binding to a broad array of phospholipids (Figure 5A), suggesting that the C1 is a
162 nonspecific phospholipid binding module.

163 To better understand the role of the C1 in aPKC polarity, we examined the effect of removing it
164 (aPKC ΔC1; Figure 5B) on aPKC's localization. We found that aPKC ΔC1 remained in the
165 cytoplasm and was not enriched at the membrane (Figure 5C-E), leading us to conclude that
166 the C1 is required for aPKC membrane targeting in NSCs. Interestingly, Mira localization was
167 also disrupted in NSCs expressing aPKC ΔC1 suggesting that the C1 also plays a role in
168 regulating aPKC's protein kinase activity in NSCs. The displacement of cortical Mira in NSCs
169 expressing aPKC ΔC1 is consistent with the increase in catalytic activity observed in *in vitro*
170 measurements of this protein (Graybill et al., 2012; Zhang et al., 2014).

171 The PS domain has been reported to be a membrane binding module required for membrane
172 recruitment of aPKC in cultured cells and epithelia (Dong et al., 2020). Our results suggest that
173 the PS is not sufficient for localization to the NSC membrane as aPKC PB1-PS remains in the
174 cytoplasm. We tested whether the PS is required for NSC aPKC membrane recruitment by
175 examining the localization of aPKC in which the positively charged, basic residues were
176 removed and a negatively charged side chain added (aPKC AADAA; Figure 5B). This mutation
177 has been reported to abrogate membrane binding in contexts where the PS is required (Dong
178 et al., 2020). We found that the apical localization of aPKC AADAA in NSCs was slightly
179 reduced compared to WT aPKC, suggesting that the PS contributes to the recruitment process
180 but is not absolutely required for recruitment or polarization in this cellular context (Figure 5C-
181 E). Mira localization was cytoplasmic in aPKC AADAA-expressing NSCs, however, consistent
182 with the increase in kinase activity that is expected when the autoinhibitory PS is inactivated
183 (Graybill et al., 2012). We also assessed the localization of aPKC AADAA in the epithelium of
184 the larval brain inner proliferation center by expressing it with the c855a-GAL4 driver. We found
185 this protein to be enriched at the apical membrane of interphase epithelial cells in a similar
186 pattern to wild-type aPKC (Figure 5F-H). We also examined the localization of the isolated C1
187 in interphase epithelial cells and observed a similar pattern to NSCs – predominantly nuclear
188 but also enriched at the membrane relative to the cytoplasm (Figure 5F-H).

189 **Regulation of membrane recruitment by the PB1 domain and its interaction with Par-6**
190 Our results indicate that recruitment of aPKC to the membrane is mediated primarily by the C1
191 domain. The constitutive membrane binding of the isolated C1 suggests that other aPKC
192 domains regulate the C1 through autoinhibition to yield the dynamic membrane localization of
193 full-length aPKC. In this model, perturbation of a regulatory domain could lead to constitutively
194 cytoplasmic or membrane-bound aPKC if the perturbation disrupted C1 activation or
195 repression, respectively. Cytoplasmic aPKC has been observed upon inactivation of aPKC's
196 PDZ Binding Motif (PBM; Holly et al., 2020), and kinase domain active site perturbations lead
197 to uniform membrane binding (Figure 1) (Hannaford et al., 2019; Rodriguez et al., 2017). We
198 determined if aPKC's PB1 domain (Figure 1A) participates in C1 regulation by examining the
199 localization of aPKC D77A, a PB1 point mutation that disrupts interaction with Par-6's PB1
200 domain (Hirano et al., 2004), and aPKC ΔPB1, which lacks the PB1 entirely (Figure 6A).
201 Intriguingly, each perturbation leads to a distinct effect – disrupting the interaction with Par-6
202 leads to cytoplasmic aPKC but complete deletion of the PB1 leads to constitutive membrane
203 binding (Figure 6B-D). The distinct localization resulting from these two perturbations indicate
204 that the PB1 is required to repress aPKC membrane recruitment and PB1's interaction with
205 Par-6 is required to overcome this regulation.

206 **Discussion**
207 The Par complex component aPKC undergoes a dynamic localization cycle in NSCs, targeting
208 to the apical membrane briefly in mitosis and returning to the cytoplasm as division completes
209 (Oon and Prehoda, 2019). The function of interphase, cytoplasmic localization is unknown, but
210 the apical localization of aPKC during mitosis is necessary for the polarization of fate
211 determinants (Atwood et al., 2007; Prehoda, 2009; Rolls et al., 2003), a prerequisite for
212 asymmetric cell division. Regulated membrane recruitment of aPKC is a central aspect of Par-
213 mediated polarity and many physical interactions between aPKC and proteins and
214 phospholipids have been identified. Conceptually, targeting could occur through the concerted
215 action of multiple weak interactions (i.e., avidity). However, we discovered that the aPKC C1
216 domain is a phospholipid binding module sufficient for membrane recruitment, whereas
217 domains that mediate protein-protein interactions or other interactions with phospholipids are
218 not sufficient for aPKC targeting. As the C1 is the only domain within aPKC with this capability
219 in NSCs, our results suggest that other aPKC domains, including the catalytic domain,
220 function, at least in part, to regulate the membrane recruitment activity of the C1. While the PS

221 and C1 domains are both known to form intramolecular interactions with the catalytic domain
222 (Graybill et al., 2012; Zhang et al., 2014), a predicted structure of aPKC suggests that there are
223 also significant intramolecular interactions within the regulatory PB1-PS-C1 module (Figure 7A)
224 (Jumper et al., 2021; Varadi et al., 2022). Taken collectively, we propose that cooperative
225 activation of the C1 leads to the spatially and temporally controlled localization of aPKC
226 observed in many animal cells.

227 The C1 is unique in its ability to promote aPKC membrane recruitment in NSCs. While
228 numerous interactions between phospholipids and domains outside the C1 have been reported
229 (Wang et al., 2005; Ivey et al., 2014; Kajimoto et al., 2019; Dong et al., 2020), our results
230 indicate that they are not sufficient for membrane recruitment in NSCs. Similarly, the domains
231 that mediate protein-protein interactions, such as the PB1 that binds Par-6 and the PBM that
232 binds Baz, are also not sufficient for aPKC recruitment. While the isolated Par-6 and aPKC PB1
233 domains bind one another *in vitro,* our data indicate that the aPKC PB1 domain is not sufficient
234 for membrane targeting, perhaps because Par-6 itself requires aPKC for membrane targeting
235 (Rolls et al., 2003).

236 The constitutive nature of C1 membrane binding raises the question of how its activity is
237 regulated to yield aPKC's precise spatially and temporally controlled localization. The aPKC
238 catalytic domain forms intramolecular interactions with the PS and C1 that repress kinase
239 activity (Graybill et al., 2012; Zhang et al., 2014), forming an "inhibitory core" (Figure 7B). Our
240 results suggest the inhibitory core is coupled to C1 membrane binding. We observed C1
241 localization at the membrane throughout the cell cycle and uniform membrane binding in
242 mitosis when aPKC is normally restricted to the apical hemisphere. We also observed
243 constitutive membrane recruitment in aPKC variants where the catalytic domain was
244 perturbed, suggesting that it is required for repression of C1 activity. We suggest that
245 perturbations to the catalytic domain that influence protein kinase activity can also disrupt the
246 inhibitory core, consistent with the complex allosteric pathways in eukaryotic protein kinase
247 domains (Ahuja et al., 2019). It has been proposed that the PS plays a central role in
248 membrane recruitment and coupling localization to the inhibitory core through its interactions
249 with the catalytic domain (Dong et al., 2020). Our results indicate that the PS is not sufficient
250 for membrane recruitment, nor is its interaction with the aPKC catalytic domain required for
251 polarization in NSCs or in a larval epithelium – aPKC AADAA is polarized but constitutively

252 active. We suggest that the PS plays a more significant role in regulating catalytic activity than
253 localization in these tissues.

254 Given that the C1 appears to be autoinhibited by the catalytic domain, how might it become
255 activated? We previously found that inactivation of the aPKC PBM (aPKC V606A), which binds
256 Baz, leads to cytoplasmic aPKC localization (Holly et al., 2020). Taken with our current results,
257 we suggest that the interaction with Baz is required for membrane recruitment not because
258 Baz directly recruits aPKC (e.g., aPKC ΔC1 is cytoplasmic), but because the Baz interaction is
259 required for disruption of the inhibitory core and activation of the C1. Similarly, in NSCs lacking
260 the PB1-binding Par-6 protein, aPKC also remains in the cytoplasm, even though Baz remains
261 properly polarized and could potentially bind aPKC's PBM (Rolls et al., 2003). These
262 observations underlie our emphasis on the cooperative nature of aPKC membrane recruitment
263 – activation of the C1 by at least Par-6 and Baz leads to the complex localization dynamics of
264 aPKC observed in NSCs. Future work will be directed at understanding how the aPKC PB1
265 and PBM might be coupled to the inhibitory core and activation of aPKC membrane binding.

266 **Materials and Methods**

267 *Drosophila*

268 Flies were grown at indicated temperatures on standard cornmeal/yeast media. Both male and
269 female larvae were used in this study. Transgenic constructs were cloned into the pUAST attB
270 vector (GenBank: EF362409.1) modified to include an N-terminal 3xHA or 1xHA tag. Integration
271 of the vectors was done using standard Phi-C31 integration into an attP landing site on the
272 third chromosome (attP2) by Rainbow Genetics or BestGene Inc. Positive insertion was
273 determined by the presence of colored eyes after backcrossing to y,w stock.
274

275 *Immunofluorescence*

276 For analysis of neural stem cells, *insc*-Gal4 virgins were crossed to males containing an aPKC
277 transgene on the third chromosome or an RNAi on the second chromosome and an aPKC
278 transgene on the third chromosome. Crosses laid in vials for 24 hours at ~20˚C. The resulting
279 embryos were incubated at 30˚C until larvae reached third instar wandering larva stage. For
280 optic lobe experiments, *c855a*-Gal4 virgins were crossed to males containing an aPKC
281 transgene on the third chromosome. Crosses laid in vials for 7 days (~20˚C) and the resulting
282 progeny were incubated at 30˚C for 24 hours. Wandering third instar larva were selected for
283 dissection. Following dissection, the tissue was incubated in 4% PFA fixative for 20' within 20'

284 of dissection. This and all subsequent wash steps involved agitation by placing on a nutator.
285 After fixation, brains were rinsed and washed three times for 15' each in PBST (1xPBS with
286 0.3% Triton-X). Brains were stored for up to three days at 4˚C before staining. Before staining,
287 brains were blocked for 30' in PBSBT (PBST with 1% BSA) and then incubated with primary
288 antibody solution overnight at 4˚C. Brains were subsequently rinsed and washed three times
289 for 15' each in PBSBT and incubated with secondary antibody for 2 hours in a vessel that
290 protected the sample from light. Brains were subsequently rinsed and washed three times for
291 15' each in PBST followed by storage in SlowFade w/DAPI at least overnight before imaging.
292 Brains were imaged on an upright Leica TCS SPE confocal using an ACS APO 40x 1.15 NA Oil
293 CS objective.
294
295 *MARCM Immunofluorescence*
296 To create MARCM larval NSC clones, FRT-G13, aPKC^{K06403}/CyO virgins were crossed with
297 3xHA aPKC D388A males. The subsequent progeny were allowed to grow to adulthood and
298 were screened for the absence of the CyO marker. Males with no CyO were then crossed to
299 elav-Gal4, UAS-mCD8:GFP, hs:flp; FRT-G13, tubPGal80 virgins.
300 Crosses laid in vials for 24 hours and the resulting embryos were incubated at room
301 temperature (~20˚C) for 24 hours. These vials were then heat shocked at 37˚C for 90 min.
302 Another heat shock was possible within 18 hours. Larvae were allowed to grow at room
303 temperature or 18˚C until third instar wandering larva stage, when they were dissected and
304 fixed as above.
305
306 *Membrane enrichment and polarization quantification*
307 A 10 pixel-wide line from apical to basal membrane in the medial optical section was used to
308 measure membrane signals in metaphase NSCs. The signal at the edge of the cell was used as

309 the membrane signal and the cytoplasmic signal was taken as the average of 20 data points
310 located 10 points from the apical peak.
311 For interphase NSCs and epithelial cells, cortical intensity was measured by tracing the cortex
312 with a 3px line, while cytoplasmic signal was taken as an average of the entire cytoplasmic
313 signal.
314 All images were analyzed using Fiji and statistical analysis was done using DABEST python
315 package (https://github.com/ACCLAB/DABEST-python).
316 Figures were assembled using Adobe Illustrator.
317
318 *Vesicle cosedimentation assay*
319 MBP-C1 was purified use amylose agarose affinity purification as previously described
320 (Graybill et al., 2012). For Giant Unilamellar Vesical (GUV) production, 50 µl of the specified
321 lipids at 10mg/mL in chloroform was dried in a test tube under an N_2 stream and then in a
322 vacuum chamber to ensure all chloroform was removed. Lipids were resuspended in a 0.2M
323 sucrose solution to a final concentration of 0.5mg/mL and heated in a water bath at 50˚C for 5
324 hours with occasional agitation. All lipids were stored at 4˚C and used within 3 days. All spins
325 were carried out using an Optima MAX-TL Ultracentrifuge with a TLA-100 rotor at 65,000 at
326 4˚C.
327 MBP-C1 protein was diluted to 50µM in 20 mM HEPES, pH 7.5; 50 mM NaCl, 1 mM DTT and
328 pre-cleared for 30'. Reaction conditions: 20mM HEPES, pH 7.5, 50mM NaCl, 1mM DTT,
329 0.25mg/mL GUVs, and 5µM MBP-C1. Reaction was carried out at room temperature for 15'
330 and then spun down for 30'. The supernatant fraction was removed, and the pellet was
331 resuspended in an equivalent volume of 1X Dilution buffer. Both the supernatant and pellet
332 samples were mixed with 6x loading dye and separated using 12.5% SDS-PAGE. Gels were
333 stained with Coomassie and imaged using a scanner.
334
335 **Key Resources Table**

Reagent type (species) or resource	Designation	Source or reference	Identifiers	Additional information
antibody	anti-aPKC	SCBT	Mouse Anti-PKC zeta (H1); SC-17781	1:1000
antibody	anti-Par-6	Alpha diagnostic	N/A	Rat Anti-Par-6 (polyclonal custom antibody); 1:500

antibody	anti-Mira	Abcam	Rat Anti-Mira; Ab197788	1:500
antibody	anti-HA	Cell Signaling Tech.	Rabbit Anti-HA (C29F4); 3724	1:1000
antibody	anti-HA	Covance	Mouse Anti-HA; MMS-101P	1:500
antibody	anti-Baz	C.Q.Doe Lab	N/A	Guinea Pig Anti-Baz (polyclonal custom antibody); 1:2000
antibody	anti-GFP	Abcam	Chicken Anti-GFP; Ab13970	1:500
antibody	anti-rat Cy3 secondary	Jackson Immuoresearch Lab.	Donkey Anti-Rat Cy3; 712-165-153	1:500
antibody	anti-rabbit 647 secondary	Jackson Immunoresearch Lab.	Donkey Anti-Rabbit 647; 711-605-152	1:500
antibody	anti-mouse 647 secondary	Jackson Immunoresearch Lab.	Donkey Anti-Mouse 647; 715-605-151	1:500
antibody	anti-mouse 488 secondary	Jackson Immunoresearch Lab.	Donkey Anti-Mouse 488; 715-545-151	1:500
antibody	anti-chicken 488 secondary	Jackson Immunoresearch Lab.	Donkey Anti-Chicken 488; 703-545-155	1:500
antibody	anti-guinea pig 405 secondary	Jackson Immunoresearch Lab.	Donkey Anti-Guinea Pig 405; 706-475-148	1:500
genetic reagent (*Drosophila melanogaster*)	*insc-GAL4*	Bloomington Drosophila Stock Center	*;insc-GAL4*	RRID:BDSC_8751
genetic reagent (*Drosophila melanogaster*)	*elav-GAL4*	Bloomington Drosophila Stock Center	*elav-Gal4, UAS-mCD8:GFP, hs:flp; FRT-G13, tubPGal80*	RRID:BDSC_5145
genetic reagent (*Drosophila melanogaster*)	*c855a-Gal4*	Bloomington Drosophila Stock Center	*;;c855a-GAL4*	RRID:BDSC_6990
genetic reagent (*Drosophila melanogaster*)	*aPKC^{K06403}*	C.Q. Doe Lab	*; FRT-G13, aPKCK^{06403}/CyO*	
genetic reagent (*Drosophila melanogaster*)	aPKC D388A	This study	;;3xHA-aPKC D388A (aPKC-PA)	

genetic reagent (*Drosophila melanogaster*)	aPKC D388A	This study	;;1xHA-aPKC D388A (aPKC-PA)	
genetic reagent (*Drosophila melanogaster*)	aPKC WT	This study	;;1xHA-aPKC 1-606 (aPKC-PA)	
genetic reagent (*Drosophila melanogaster*)	aPKC K293W	This study	;;1xHA-aPKC K293W (aPKC-PA)	
genetic reagent (*Drosophila melanogaster*)	aPKC PB1-C1	This study	;;1xHA-aPKC 1-195 (aPKC-PA)	
genetic reagent (*Drosophila melanogaster*)	aPKC PB1-PS	This study	;;1xHA-aPKC 1-141 (aPKC-PA)	
genetic reagent (*Drosophila melanogaster*)	aPKC C1	This study	;;1xHA-aPKC 139-195 (aPKC-PA)	
genetic reagent (*Drosophila melanogaster*)	aPKC ΔC1	This study	;;1xHA-aPKC 1-606 Δ141-196 (aPKC-PA)	
genetic reagent (*Drosophila melanogaster*)	aPKC AADAA	This study	;;1xHA-aPKC R131A, R132A, A134D, R135A, R136A (aPKC-PA)	
genetic reagent (*Drosophila melanogaster*)	aPKC ΔPB1	This study	;;1xHA-aPKC 107-606 (aPKC-PA)	
genetic reagent (*Drosophila melanogaster*)	aPKC D77A	This study	;;1xHA-aPKC D77A (aPKC-PA)	
genetic reagent (*Drosophila melanogaster*)	Baz RNAi	Bloomington Drosophila Stock Center	*;UAS-Baz RNAi*	RRID:BDSC_39072
genetic reagent (*Drosophila melanogaster*)	Cdc42 RNAi	Bloomington Drosophila Stock Center	*;UAS-Cdc42 RNAi*	RRID:VDRC_100794
chemical compound, drug	Amylose Resin	NEB	E8021L	
chemical compound, drug	Schneider's Insect Medium (SIM)	Sigma	S0146	
chemical compound, drug	SlowFade Diamond Antifade Mountant with DAPI	Invitrogen	S36964	
chemical compound, drug	Phosphatidylserine (PS)	Avanti Polar Lipids	L-α-phosphatidylserine; 840032C	

chemical compound, drug	Phosphatidylcholine (PC)	Avanti Polar Lipids	L-α-phosphatidylcholine; 840051C	
chemical compound, drug	Phosphatidic acid (PA)	Avanti Polar Lipids	L-α-phosphatidic acid; 840101C	
chemical compound, drug	Phosphatidylglycerol (PG)	Avanti Polar Lipids	L-α-phosphatidylglycerol; 841138P	
chemical compound, drug	ceramide	Avanti Polar Lipids	C12 ceramide; 860512P	

References

Ahuja LG, Taylor SS, Kornev AP. 2019. Tuning the "violin" of protein kinases: The role of dynamics-based allostery. *IUBMB Life* **71**:685–696. doi:10.1002/iub.2057

Atwood SX, Chabu C, Penkert RR, Doe CQ, Prehoda KE. 2007. Cdc42 acts downstream of Bazooka to regulate neuroblast polarity through Par-6 aPKC. *J Cell Sci* **120**:3200–3206. doi:10.1242/jcs.014902

Atwood SX, Prehoda KE. 2009. aPKC phosphorylates Miranda to polarize fate determinants during neuroblast asymmetric cell division. *Curr Biol CB* **19**:723–729. doi:10.1016/j.cub.2009.03.056

Bailey MJ, Prehoda KE. 2015. Establishment of Par-Polarized Cortical Domains via Phosphoregulated Membrane Motifs. *Dev Cell* **35**:199–210. doi:10.1016/j.devcel.2015.09.016

Colón-González F, Kazanietz MG. 2006. C1 domains exposed: from diacylglycerol binding to protein-protein interactions. *Biochim Biophys Acta* **1761**:827–837. doi:10.1016/j.bbalip.2006.05.001

Dong W, Lu J, Zhang X, Wu Y, Lettieri K, Hammond GR, Hong Y. 2020. A polybasic domain in aPKC mediates Par6-dependent control of membrane targeting and kinase activity. *J Cell Biol* **219**:e201903031. doi:10.1083/jcb.201903031

Graybill C, Wee B, Atwood SX, Prehoda KE. 2012. Partitioning-defective protein 6 (Par-6) activates atypical protein kinase C (aPKC) by pseudosubstrate displacement. *J Biol Chem* **287**:21003–21011. doi:10.1074/jbc.M112.360495

Hannaford M, Loyer N, Tonelli F, Zoltner M, Januschke J. 2019. A chemical-genetics approach to study the role of atypical Protein Kinase C in Drosophila. *Dev Camb Engl* **146**:dev170589. doi:10.1242/dev.170589

Hirano Y, Yoshinaga S, Ogura K, Yokochi M, Noda Y, Sumimoto H, Inagaki F. 2004. Solution structure of atypical protein kinase C PB1 domain and its mode of interaction with ZIP/p62 and MEK5 **279**:31883–31890. doi:10.1074/jbc.M403092200

Holly RW, Jones K, Prehoda KE. 2020. A Conserved PDZ-Binding Motif in aPKC Interacts with Par-3 and Mediates Cortical Polarity. *Curr Biol CB* **30**:893-898.e5. doi:10.1016/j.cub.2019.12.055

Homem CCF, Knoblich JA. 2012. Drosophila neuroblasts: a model for stem cell biology **139**:4297–4310. doi:10.1242/dev.080515

Ikeshima-Kataoka H, Skeath JB, Nabeshima Y, Doe CQ, Matsuzaki F. 1997. Miranda directs Prospero to a daughter cell during Drosophila asymmetric divisions. *Nature* **390**:625–629. doi:10.1038/37641

372 Ivey RA, Sajan MP, Farese RV. 2014. Requirements for pseudosubstrate arginine residues
373 during autoinhibition and phosphatidylinositol 3,4,5-$(PO_4)_3$-dependent activation of
374 atypical PKC. *J Biol Chem* **289**:25021–25030. doi:10.1074/jbc.M114.565671
375 Joberty G, Petersen C, Gao L, Macara IG. 2000. The cell-polarity protein Par6 links Par3 and
376 atypical protein kinase C to Cdc42. *Nat Cell Biol* **2**:531–539. doi:10.1038/35019573
377 Jumper J, Evans R, Pritzel A, Green T, Figurnov M, Ronneberger O, Tunyasuvunakool K, Bates
378 R, Žídek A, Potapenko A, Bridgland A, Meyer C, Kohl SAA, Ballard AJ, Cowie A,
379 Romera-Paredes B, Nikolov S, Jain R, Adler J, Back T, Petersen S, Reiman D, Clancy E,
380 Zielinski M, Steinegger M, Pacholska M, Berghammer T, Bodenstein S, Silver D, Vinyals
381 O, Senior AW, Kavukcuoglu K, Kohli P, Hassabis D. 2021. Highly accurate protein
382 structure prediction with AlphaFold. *Nature* **596**:583–589. doi:10.1038/s41586-021-
383 03819-2
384 Kajimoto T, Caliman AD, Tobias IS, Okada T, Pilo CA, Van A-AN, Andrew McCammon J,
385 Nakamura S-I, Newton AC. 2019. Activation of atypical protein kinase C by sphingosine
386 1-phosphate revealed by an aPKC-specific activity reporter. *Sci Signal* **12**:eaat6662.
387 doi:10.1126/scisignal.aat6662
388 Krahn MP, Klopfenstein DR, Fischer N, Wodarz A. 2010. Membrane targeting of Bazooka/PAR-
389 3 is mediated by direct binding to phosphoinositide lipids. *Curr Biol CB* **20**:636–642.
390 doi:10.1016/j.cub.2010.01.065
391 Lang CF, Munro E. 2017. The PAR proteins: from molecular circuits to dynamic self-stabilizing
392 cell polarity. *Dev Camb Engl* **144**:3405–3416. doi:10.1242/dev.139063
393 Lin D, Edwards AS, Fawcett JP, Mbamalu G, Scott JD, Pawson T. 2000. A mammalian PAR-3-
394 PAR-6 complex implicated in Cdc42/Rac1 and aPKC signalling and cell polarity. *Nat*
395 *Cell Biol* **2**:540–547. doi:10.1038/35019582
396 Nance J, Zallen JA. 2011. Elaborating polarity: PAR proteins and the cytoskeleton. *Dev Camb*
397 *Engl* **138**:799–809. doi:10.1242/dev.053538
398 Oon CH, Prehoda KE. 2019. Asymmetric recruitment and actin-dependent cortical flows drive
399 the neuroblast polarity cycle. *eLife* **8**. doi:10.7554/eLife.45815
400 Perander M, Bjorkoy G, Johansen T. 2001. Nuclear import and export signals enable rapid
401 nucleocytoplasmic shuttling of the atypical protein kinase C lambda. *J Biol Chem*
402 **276**:13015–13024. doi:10.1074/jbc.M010356200
403 Petronczki M, Knoblich JA. 2001. DmPAR-6 directs epithelial polarity and asymmetric cell
404 division of neuroblasts in Drosophila. *Nat Cell Biol* **3**:43–49. doi:10.1038/35050550
405 Prehoda KE. 2009. Polarization of Drosophila neuroblasts during asymmetric division. *Cold*
406 *Spring Harb Perspect Biol* **1**:a001388. doi:10.1101/cshperspect.a001388
407 Rodriguez J, Peglion F, Martin J, Hubatsch L, Reich J, Hirani N, Gubieda AG, Roffey J,
408 Fernandes AR, St Johnston D, Ahringer J, Goehring NW. 2017. aPKC Cycles between
409 Functionally Distinct PAR Protein Assemblies to Drive Cell Polarity. *Dev Cell* **42**:400-
410 415.e9. doi:10.1016/j.devcel.2017.07.007
411 Rolls MM, Albertson R, Shih H-P, Lee C-Y, Doe CQ. 2003. Drosophila aPKC regulates cell
412 polarity and cell proliferation in neuroblasts and epithelia. *J Cell Biol* **163**:1089–1098.
413 doi:10.1083/jcb.200306079
414 Seidl S, Braun UB, Leitges M. 2012. Functional comparison of protein domains within aPKCs
415 involved in nucleocytoplasmic shuttling. *Biol Open* **1**:436–445. doi:10.1242/bio.2012505
416 Smith CA, Lau KM, Rahmani Z, Dho SE, Brothers G, She YM, Berry DM, Bonneil E, Thibault P,
417 Schweisguth F, Le Borgne R, McGlade CJ. 2007. aPKC-mediated phosphorylation
418 regulates asymmetric membrane localization of the cell fate determinant Numb. *EMBO*
419 *J* **26**:468–480. doi:10.1038/sj.emboj.7601495

420 Standaert ML, Galloway L, Karnam P, Bandyopadhyay G, Moscat J, Farese RV. 1997. Protein
421 kinase C-zeta as a downstream effector of phosphatidylinositol 3-kinase during insulin
422 stimulation in rat adipocytes. Potential role in glucose transport **272**:30075–30082.
423 Tepass U. 2012. The Apical Polarity Protein Network in Drosophila Epithelial Cells: Regulation
424 of Polarity, Junctions, Morphogenesis, Cell Growth, and Survival **28**:655–685.
425 doi:10.1146/annurev-cellbio-092910-154033
426 Varadi M, Anyango S, Deshpande M, Nair S, Natassia C, Yordanova G, Yuan D, Stroe O, Wood
427 G, Laydon A, Žídek A, Green T, Tunyasuvunakool K, Petersen S, Jumper J, Clancy E,
428 Green R, Vora A, Lutfi M, Figurnov M, Cowie A, Hobbs N, Kohli P, Kleywegt G, Birney
429 E, Hassabis D, Velankar S. 2022. AlphaFold Protein Structure Database: massively
430 expanding the structural coverage of protein-sequence space with high-accuracy
431 models. *Nucleic Acids Res* **50**:D439–D444. doi:10.1093/nar/gkab1061
432 Venkei ZG, Yamashita YM. 2018. Emerging mechanisms of asymmetric stem cell division. *J*
433 *Cell Biol*. doi:10.1083/jcb.201807037
434 Wang G, Silva J, Krishnamurthy K, Tran E, Condie BG, Bieberich E. 2005. Direct binding to
435 ceramide activates protein kinase Czeta before the formation of a pro-apoptotic
436 complex with PAR-4 in differentiating stem cells. *J Biol Chem* **280**:26415–26424.
437 doi:10.1074/jbc.M501492200
438 Wodarz A, Ramrath A, Grimm A, Knust E. 2000. Drosophila atypical protein kinase C
439 associates with Bazooka and controls polarity of epithelia and neuroblasts. *J Cell Biol*
440 **150**:1361–1374. doi:10.1083/jcb.150.6.1361
441 Zhang H, Neimanis S, Lopez-Garcia LA, Arencibia JM, Amon S, Stroba A, Zeuzem S, Proschak
442 E, Stark H, Bauer AF, Busschots K, Jørgensen TJD, Engel M, Schulze JO, Biondi RM.
443 2014. Molecular mechanism of regulation of the atypical protein kinase C by N-terminal
444 domains and an allosteric small compound. *Chem Biol* **21**:754–765.
445 doi:10.1016/j.chembiol.2014.04.007
446

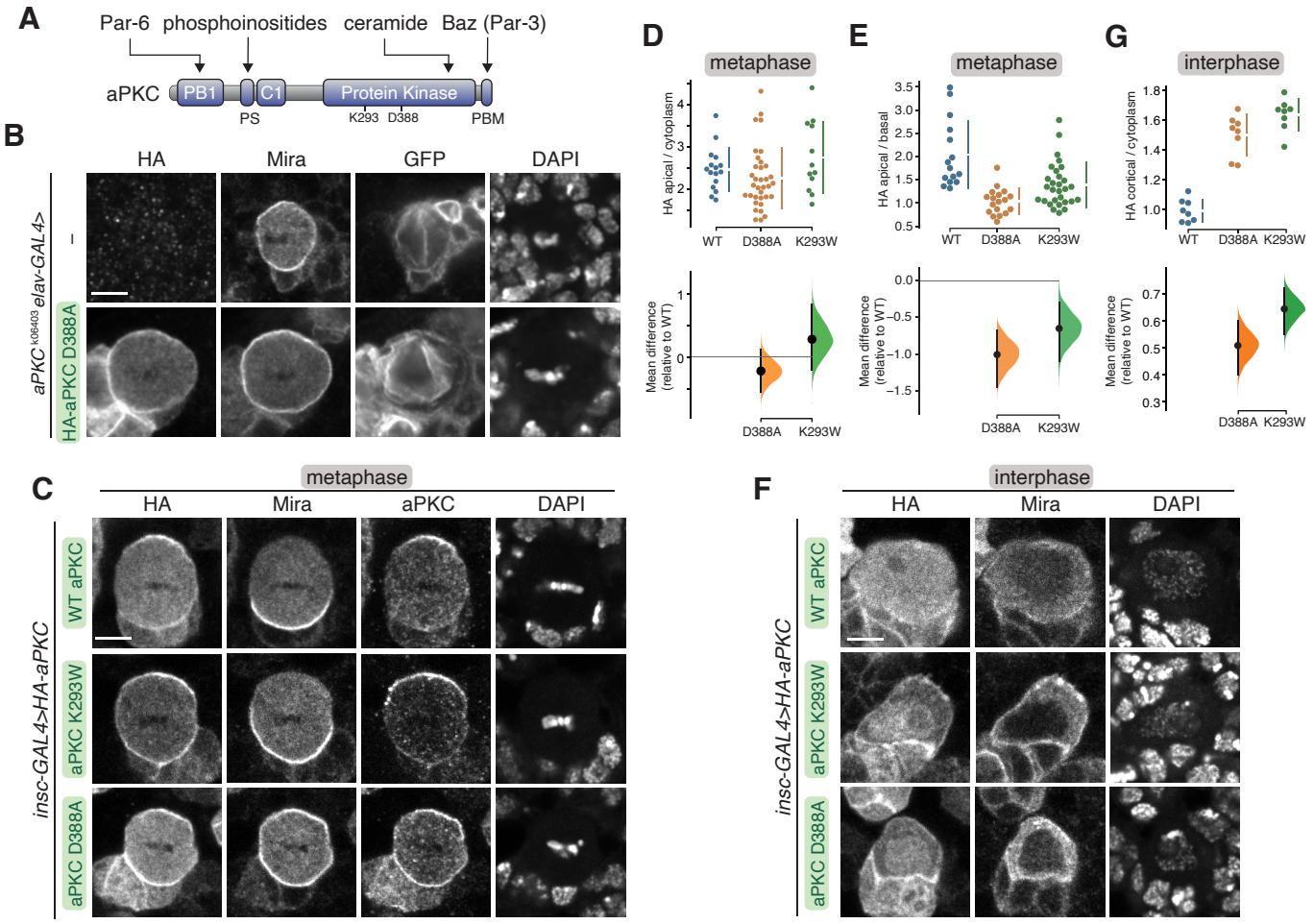

Figure 1 Localization of aPKC with kinase inactivating mutations in larval brain NSCs

(A) Domain structure of aPKC showing the location of PB1, PS (pseudosubstrate), C1, kinase domain, PBM (PDZ binding motif), along with location of K293 and D388 residues.

(B) Localization of HA tagged aPKC harboring the D388A kinase inactivating mutation in a metaphase, positively marked (mCD8-GFP) *aPKC*^{k06403} mutant larval brain NSC with an *aPKC*^{K06403} mutant larval brain NSC shown for comparison. Nucleic acids are shown with DAPI. Scale bar is 5 μm in all panels.

(C) Localization of HA tagged aPKC harboring either the D388A or K293W kinase inactivation mutations in metaphase larval brain NSCs with endogenous aPKC. The basal cortical marker Miranda, total aPKC ("aPKC", endogenous and exogenously expressed), and nucleic acid (DAPI) are also shown.

(D,E) Gardner-Altman estimation plots of the effect of the D388A and K293W mutations on metaphase aPKC membrane recruitment. Apical cortical to cytoplasmic (D) and apical/basal (ED) signal intensities of anti-HA signals are shown for individual metaphase NSCs expressing either HA-WT or HA-D388A or HA-K293W aPKC. Error bar in upper graph represents one standard deviation (gap is mean); error bar in lower graph represents bootstrap 95% confidence interval.

(F) Localization of HA tagged aPKC harboring either the D388A or K293W kinase inactivation mutations in interphase larval brain NSCs with endogenous aPKC. The basal cortical marker Miranda and nucleic acid (DAPI) are also shown.

(G) Gardner-Altman estimation plot of the effect of the D388A and K293W mutations on interphase aPKC membrane recruitment. Cortical to cytoplasmic cortical signal intensities of anti-HA signals are shown for individual metaphase NSCs expressing either HA-WT or HA-D388A or HA-K293W aPKC. Error bar in upper graph represents one standard deviation (gap is mean); error bar in lower graph represents bootstrap 95% confidence interval.

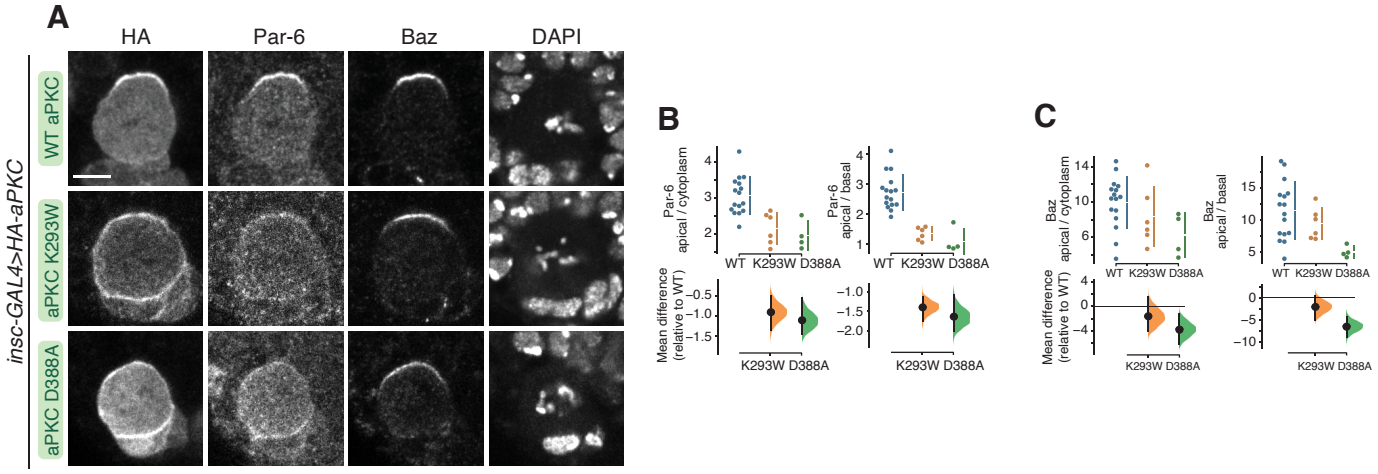

Figure 2 Localization of Bazooka and Par-6 in larval brain NSCs expressing kinase inactive aPKCs
(A) Localization of Par-6 and Bazooka (Baz) in metaphase larval brain NSCs expressing HA tagged aPKC D388A or aPKC K293W. Nucleic acids are shown with DAPI. Scale bar is 5 μm.
(B,C) Gardner-Altman estimation plots of the effect of expressing aPKC D388A or aPKC K293W on Par-6 (B) or Baz (C) cortical localization and polarity. Apical cortical to cytoplasmic or basal cortical signal intensities of cortical and cytoplasmic signals are shown for individual metaphase NSCs expressing either HA-WT or HA-D388A or HA-K293W aPKC. Error bar in upper graphs represents one standard deviation (gap is mean); error bar in lower graphs represents bootstrap 95% confidence interval.

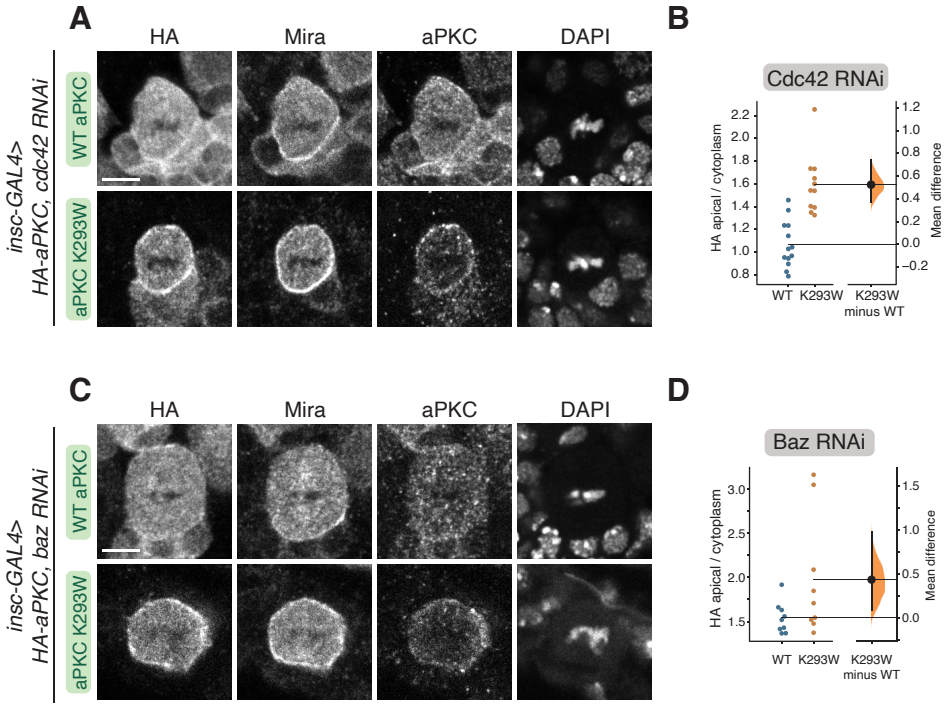

Figure 3 Cortical localization of kinase inactive aPKC in NSCs lacking Bazooka or Cdc42
(A) Localization of HA tagged aPKC K293W in metaphase larval brain NSCs expressing an RNAi directed against Cdc42. Scale bar is 5 μm in all panels.
(B) Gardner-Altman estimation plots of the effect of expressing Cdc42 RNAi on WT and K293W aPKC cortical localization. Apical cortical to cytoplasmic signal intensities of anti-HA signals are shown for individual metaphase NSCs expressing either HA-WT or HA-K293W aPKC. Error bar represents bootstrap 95% confidence interval.
(C) Localization of HA tagged aPKC K293W in metaphase larval brain NSCs expressing an RNAi directed against Bazooka.
(D) Gardner-Altman estimation plots of the effect of expressing Baz RNAi on WT and K293W aPKC cortical localization. Apical cortical to cytoplasmic signal intensities of anti-HA signals are shown for individual metaphase NSCs expressing either HA-WT or HA-K293W aPKC. Error bar represents bootstrap 95% confidence interval.

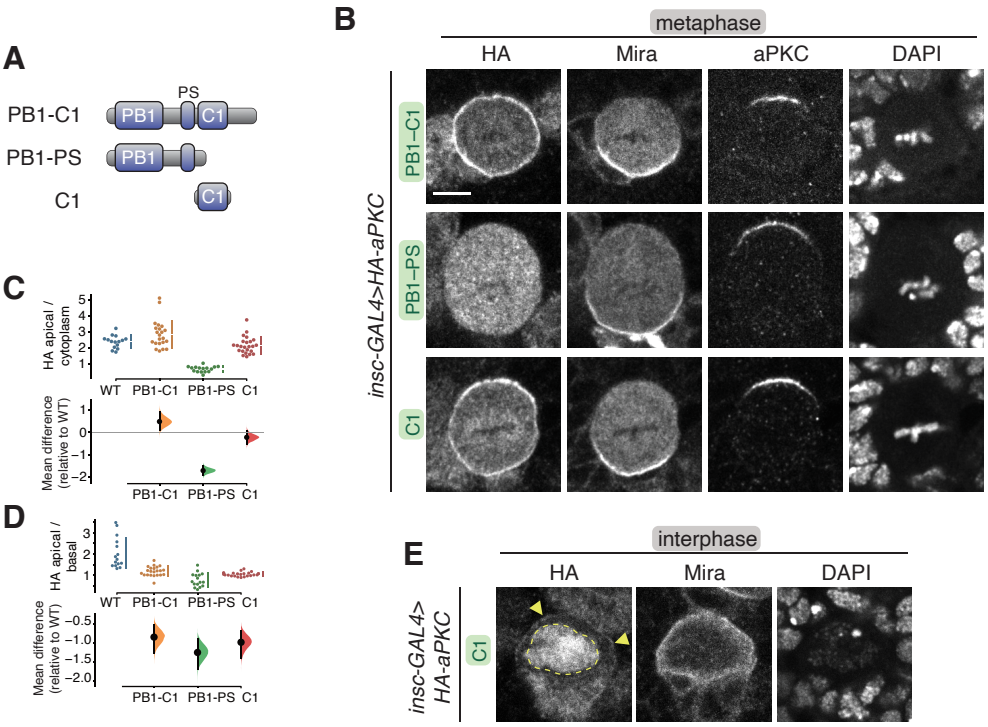

Figure 4 Localization of the aPKC regulatory domain in larval brain NSCs
(A) aPKC regulatory domain fragments.
(B) Localization of HA tagged aPKC regulatory domain fragments in metaphase larval brain NSCs. The basal marker Miranda, endogenous aPKC (using an antibody that does not react with the regulatory domain), nucleic acids (DAPI) are shown for comparison. Scale bar is 5 μm.
(C,D) Gardner-Altman estimation plot of aPKC regulatory domain cortical localization (C) and polarity (D). Apical cortical to cytoplasmic (C) and apical cortical to basal cortical signal intensity ratios (D) of anti-HA signals are shown for individual metaphase NSCs expressing either aPKC PB1-C1, PB1-PS, or C1 regulatory domain fragments. Error bar in upper graphs represents one standard deviation (gap is mean); error bar in lower graphs represents bootstrap 95% confidence interval.
(E) Localization of the HA tagged aPKC C1 domain in interphase larval brain NSCs. Arrowheads highlight the membrane signal and the nuclear signal is outlined by a dashed line.

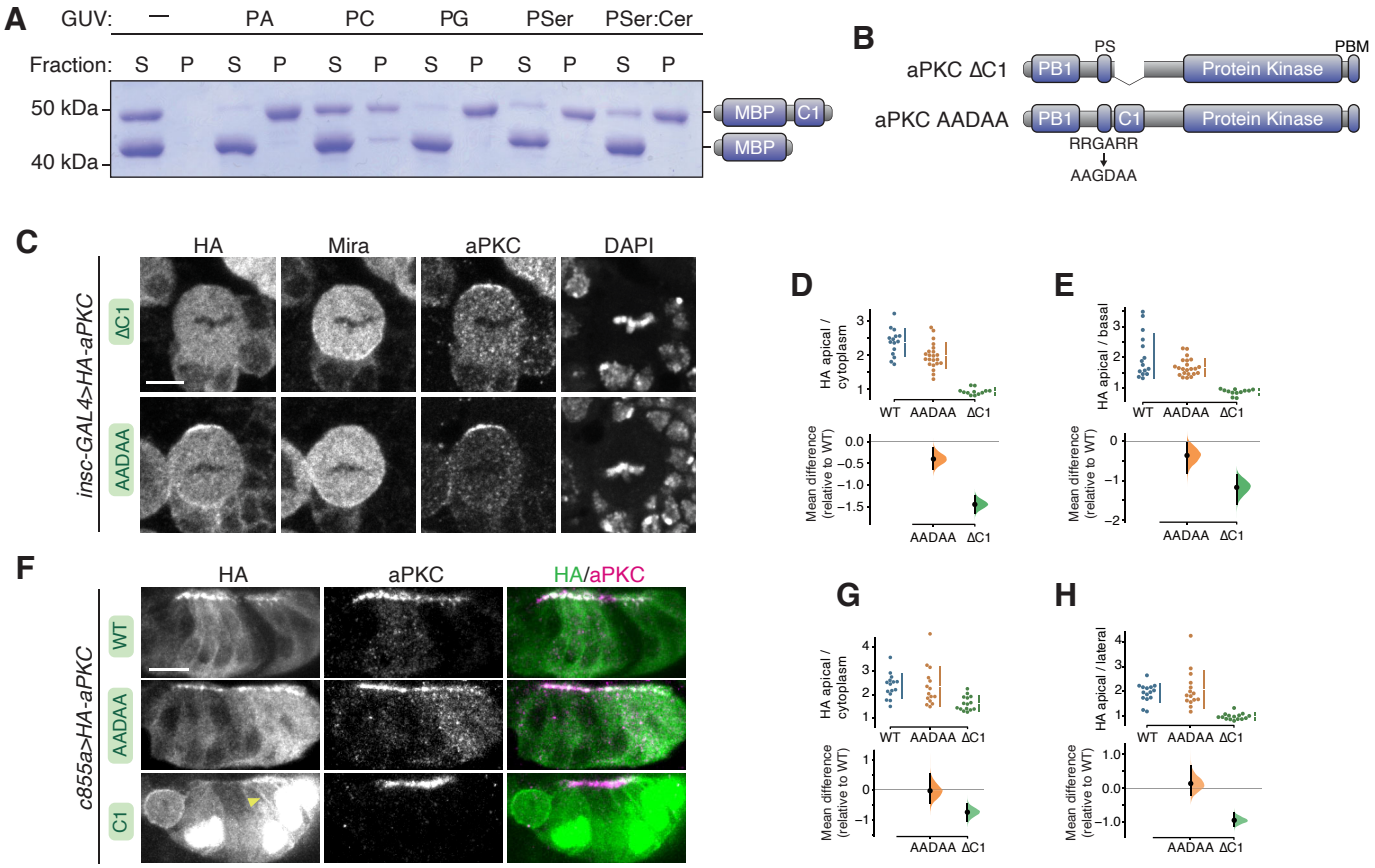

Figure 5 Phospholipid binding of aPKC C1 domain and role of C1 and PS domains in aPKC localization in larval brain NSCs and epithelia

(A) Binding of a maltose binding protein (MBP) fusion of the aPKC C1 domain to phospholipids. Supernatant (S) and pellet (P) fractions from cosedimentation with Giant Unilamellar Vesicles (GUVs) of the indicated phospholipid composition are shown (PA, phosphatidic acid; PC, phosphatidyl choline; PG, phosphatidyl glycerol; PSer, phosphatidyl serine; PSer:Cer, phosphatidyl serine mixture with ceramide). MBP alone is included as an internal negative control.

(B) Schematics of ΔC1 and AADAA aPKC variants.

(C) Localization of HA tagged aPKC ΔC1 and AADAA variants in metaphase larval brain NSCs. The basal marker Miranda, total aPKC (expressed variant and endogenous), nucleic acids (DAPI) are shown for comparison. Scale bar is 5 μm.

(D,E) Gardner-Altman estimation plots of aPKC AADAA and ΔC1 cortical localization in NSCs. Apical cortical to cytoplasmic (D) or apical to basal (E) signal intensity ratios of anti-HA signals are shown for individual metaphase NSCs expressing either aPKC AADAA or ΔC1. Error bar in upper graphs represents one standard deviation (gap is mean); error bar in lower graphs represents bootstrap 95% confidence interval.

(F) Localization of HA tagged aPKC ΔC1 and AADAA variants in larval brain inner proliferation center (IPC) epithelium. Arrowhead highlights aPKC C1 localization at the lateral membrane. As in interphase NSC cells, the C1 is highly enriched in the epithelial nuclei. Scale bar is 5 μm.

(G,H) Gardner-Altman estimation plots of aPKC AADAA and C1 cortical localization in IPC epithelial cells. Apical cortical to cytoplasmic (D) or apical to lateral (E) signal intensity ratios of anti-HA signals are shown for individual epithelial cells from the IPC expressing either aPKC AADAA or C1. Error bar in upper graphs represents one standard deviation (gap is mean); error bar in lower graphs represents bootstrap 95% confidence interval.

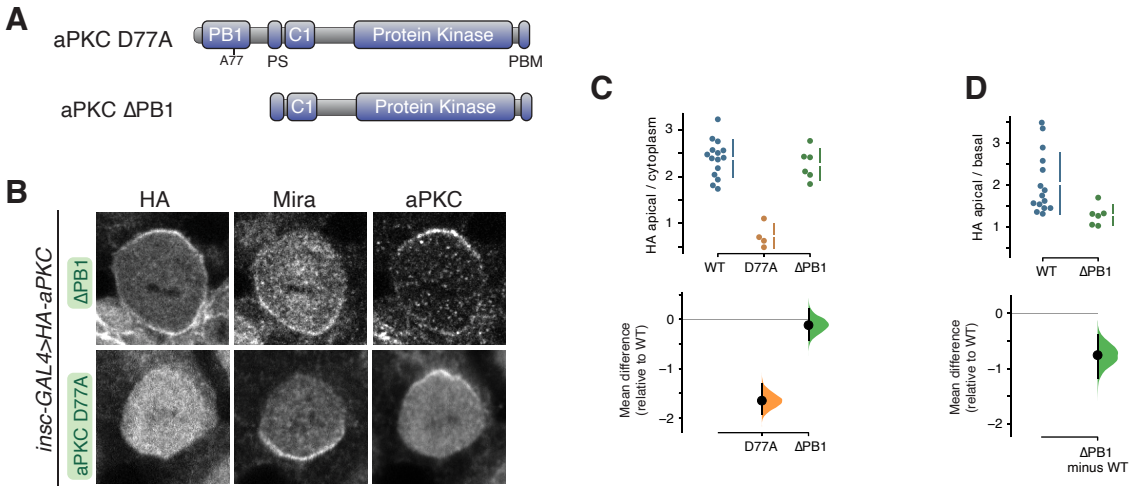

Figure 6 Localization of aPKC with PB1 domain perturbations in larval brain NSCs
(A) Schematics of D77A and ΔPB1 aPKC variants.
(B) Localization of HA tagged aPKC D77A and ΔPB1 variants in metaphase larval brain NSCs. The basal marker Miranda, and total aPKC (expressed variant and endogenous), are shown for comparison. Scale bar is 5 μm.
(C,D) Gardner-Altman estimation plots of aPKC D77A and ΔPB1 cortical localization. Apical cortical to cytoplasmic (C) or apical to basal (D) signal intensity ratios of anti-HA signals are shown for individual metaphase NSCs expressing either aPKC D77A or ΔPB1. Error bar in upper graphs represents one standard deviation (gap is mean); error bar in lower graphs represents bootstrap 95% confidence interval.

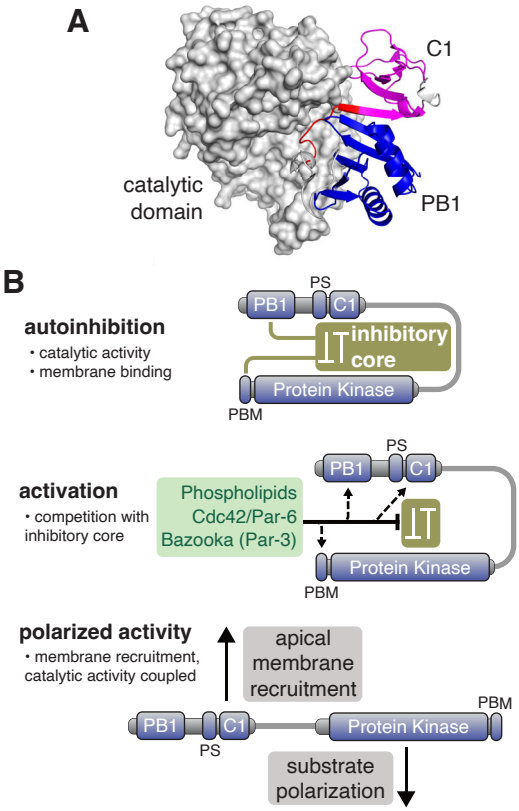

Figure 7 Model for regulation of aPKC activity and membrane recruitment
(A) Alphafold database structure (UNIPROT: A1Z9X0) of aPKC showing putative supramolecular architecture of PB1 (blue), PS (red) and C1 (magenta) domains and interaction of both domains with the catalytic domain.
(B) Model for cooperative polarization and activation of aPKC. An inhibitory core couples repression of catalytic activity (protein kinase domain) to membrane localization (C1 with some contribtion from PS). The PB1 and PBM are also coupled to the inhibitory core to allow for cooperative activation by Cdc42/Par-6 binding to the PB1 and Baz binding to the PBM. Disruption of the inhibitory core leads to spatially (apical) and temporally (mitotic) regulated localization and activation of catalytic activity.